International Journal of Biological Macromolecules 266 (2024) 131405

Contents lists available at ScienceDirect

International Journal of Biological Macromolecules

journal homepage: www.elsevier.com/locate/ijbiomac

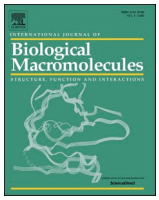

Binding mechanism of pentamidine derivatives with human serum acute phase protein α_1-acid glycoprotein

Teresa Żołek [a,*], Orsolya Dömötör [b], Jerzy Żabiński [a]

[a] Department of Organic and Physical Chemistry, Faculty of Pharmacy, Medical University of Warsaw, Banacha 1, 02-097 Warsaw, Poland
[b] Department of Molecular and Analytical Chemistry, Interdisciplinary Excellence Centre, University of Szeged, Dóm tér 7-8, 6720 Szeged, Hungary

ARTICLE INFO

Keywords:
Pentamidine derivatives
α_1-acid glycoprotein interactions
Spectrofluorometric
Proton dissociation constants and lipophilicity
Computational modelling

ABSTRACT

Drug binding and interactions with plasma proteins play a crucial role in determining the efficacy of drug delivery, thus significantly impacting the overall pharmacological effect. AGP, the second most abundant plasma protein in blood circulation, has the unique capability to bind drugs and transport various compounds. In our present study, for the first time, we investigated whether AGP, a major component of the acute phase lipocalin in human plasma, can bind with pentamidine derivatives known for their high activity against the fungal pathogen *Pneumocystis carinii*. This investigation was conducted using integrated spectroscopic techniques and computer-based approaches. According to the results, it was concluded that compounds having heteroatoms (-NCH_3) in the aliphatic linker and the addition of a —Br atom and a methoxy substituent at the C-2 and C-6 positions on the benzene ring, exhibit strong interactions with the AGP binding site. These compounds are identified as potential candidates for recognition by this protein. MD studies indicated that the tested analogues complexed with AGPs reach an equilibrium state after 60 ns, suggesting the stability of the complexes. This observation was further corroborated by experimental results. Therefore, exploring the interaction mechanism of pentamidine derivatives with plasma proteins holds promise for the development of *bis*-benzamidine-designed pharmaceutically important drugs.

1. Introduction

The interaction of drugs or small molecules with plasma proteins is considered an important determinant of their effective distribution to various organs or sites of action within the body. Many drugs are transported and distributed in the bloodstream either in a free form or bound to plasma proteins. Unlike the free portion, the protein-bound fraction of the active substance is not subject to metabolic processes and premature excretion. Therefore, the binding of drugs and drug candidates to plasma proteins is an important factor influencing their pharmacokinetics and pharmacodynamics [1]. Blood plasma contains many proteins and factors (e.g., albumins, globulins, fibrinogen) involved in many physiological and pathological functions, including the transport of endogenous or exogenous molecules. Among these plasma proteins, drugs mostly bind to human serum albumin (HSA), the most predominant protein and a negative acute phase protein in the blood. Additionally, drugs bind to a significant extent to human α_1-acid glycoprotein (AGP), which is a positive acute phase protein [2,3]. Despite constituting a relatively small amount of total plasma protein (approximately 1–3 %), AGP has unique saturable and displaceable drug-binding properties [4].

AGP is an acute phase protein whose blood levels are elevated in inflammatory processes, various forms of cancer and infections, as well as in pregnancy and following major surgical interventions [5]. The normal level of AGP in plasma from ranges 0.6 to 1.2 mg/ml (14–29 μM), but this can increase 2 to 5 times in patients experiencing inflammation and malignancies. Notably, changes in AGP concentration in plasma can significantly impact the fraction of drugs bound at their target site, thus potentially altering the pharmacokinetics and pharmacodynamics of drugs [6,7]. This means that under acute phase conditions, there is a risk that the free fraction of the strongly protein-bound drugs may not reach the therapeutic concentration. As a member of the lipocalin protein family, AGP possesses three tryptophan residues (Trp-25, Trp-122 and Trp-160) and a large central hydrophobic cavity, which is the main binding region for a variety of ligands ranging from small inorganic anions to steroid hormones and a variety of drugs, especially neutral and basic compounds [8,9]. The interaction of ligands with AGP can be assessed by monitoring changes in fluorescence emission, which

* Corresponding author.
E-mail address: tzolek@wum.edu.pl (T. Żołek).

https://doi.org/10.1016/j.ijbiomac.2024.131405
Received 18 February 2024; Received in revised form 2 April 2024; Accepted 3 April 2024
Available online 4 April 2024
0141-8130/© 2024 The Authors. Published by Elsevier B.V. This is an open access article under the CC BY license (http://creativecommons.org/licenses/by/4.0/).

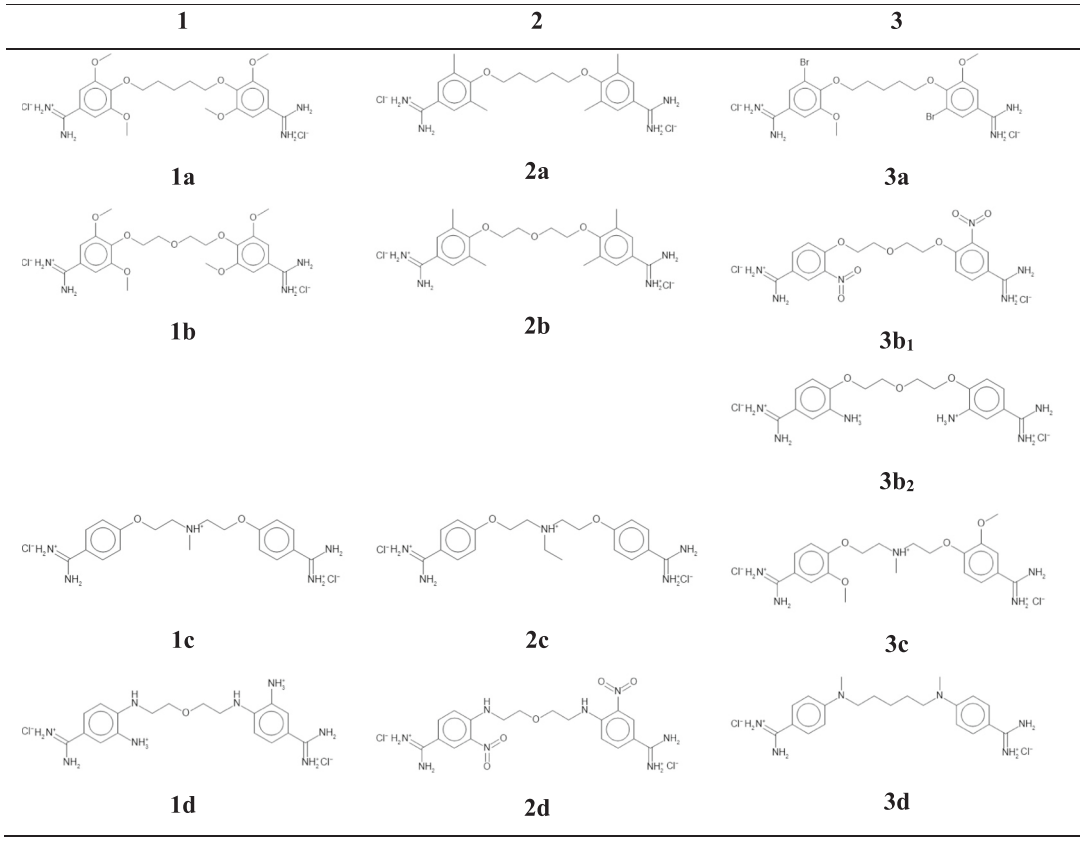

Fig. 1. Chemical structures of thirteen pentamidine derivatives.

arise from the presence of the three Trp residues. AGP, also known as orosomucoid, is composed of 183 amino acid residues and contains five to six *N*-linked oligosaccharides corresponding to a molecular weight of 41–43 kDa. It is heavily glycosylated consisting of about 40 % carbohydrate content by weight. The high content of sialic acids at the glycan terminals (about 12 %) contributes to its low isoelectric point (pI) of 2.8–3.8 [5] and is also responsible for stereoselectivity in the binding of basic drugs [10]. Given this, the study of binding interactions between AGP and drugs has garnered significant attention, as it could contribute to drug discovery and development by providing information about those structural features that determine the therapeutic effect of drugs [6]. The binding interaction has been reported for a wide range of drugs/ligands, including colistin, polymyxin B, colistin methanesulfonate, mifepristone, *N*-acetylneuraminic acid, warfarin, tamsulosin, clofarabine, cabozantinib, tofacitinib, piperine, imatinib, 6-mercaptopurine, thymoquinone, etc. [11–15]. However, based on available literature data, we noticed that the binding of *bis*-benzamidines to AGP has not yet been described.

The benzamidine moiety is a significant pharmacophore in the discovery of new derivatives with novel biological properties. The *bis*-benzamidines have been reported to display a diverse group of compounds with great potential in pharmacotherapy. Among these, pentamidine stands out as a drug of great therapeutic importance in the prevention and treatment of infectious diseases from *Pneumocystis jiroveci* pneumonia (PJP) to human African trypanosomiasis (HAT) [16–20]. Apart from its antiprotozoal activity, pentamidine exhibits moderate antibacterial activity against gram-positive species [21,22]. Furthermore, pentamidine has been demonstrated to possess anticancer activity by restoring the tumor-suppressive activity of p53. It can also bind to A-T-rich regions of double-stranded DNA and non-specifically bind to and disrupt secondary tRNA structures [23–26]. Pentamidine is currently in phase II clinical trials in refractory melanoma. However, despite its clinical usefulness, it has many toxic side effects and low bioavailability [27]. The results of many studies indicated that the electron and conformational nature of the linker can influence not only the chemical properties of the amidine moieties but also improve the biological activity of the pentamidine derivatives [28–30]. Among them, furamidine, a *bis*-amidine diphenylfuran, exhibited significant against PJP and antiprotozoal activities [31], while a series of cyclic dibenzamidines with triazine and carbazole linkers, as well as furamidine derivatives characterized by different structural features, have displayed activities against a broad panel of tumor cell lines [32,33]. Recent years have witnessed intensive work in many research centers, including our own, focusing on the synthesis, in vitro testing, or clinical trials of several pentamidine derivatives featuring modified chain structures connecting various cationic groups. However, despite these efforts, the quest for new compounds with greater bioavailability, more effective and less toxic than pentamidine remains ongoing [22,34–36]. Perhaps, the efficacy and toxicity of pentamidine are closely related to its binding with plasma proteins, especially the binding of basic drugs with AGP. Therefore, the idea arose to support this search by monitoring the interactions of several pentamidine derivatives (see Fig. 1) with AGP. This approach is anticipated to provide important information for the early evaluation of new pentamidine derivatives showing in vitro therapeutic efficacy. Our research group synthesized thirteen compounds with different heteroatoms in the aliphatic linker (O and N) and varying functional groups on the benzene rings [37,38], which belong to linear pentamidine analogues. These compounds were subjected to analysis in our study. All compounds exhibited high activities, with IC_{50} values ranging from 0.01 to 3.4 μM, in mammalian cell lines during the test using *Pneumocystis carinii* organisms and the ATP bioluminescent assay. Additionally, none of the compounds showed cytotoxicity.

In our recent study, we demonstrated that related pentamidine ligands did not significantly bind to HSA [39]. Considering that HSA

prefers binding negatively charged and neutral small molecules at its three hydrophobic binding sites (Sudlow sites I and II and a third site in subdomain IB), our interest turned towards studying the binding of molecules to AGP. The purpose of this study is to obtain biophysical insight into the interaction characteristics of pentamidine derivatives with AGP. This includes assessing their binding affinity ability through multiple spectroscopic techniques (UV–visible (UV–vis) spectrophotometric and spectrofluorometric), as well as determining distribution coefficients (D_{pH}) and proton dissociation constants (pK_a) combined with computational techniques (molecular docking and molecular dynamics simulation) to locate the binding region of pentamidine derivatives on AGP molecule and elucidate information their thermodynamic and dynamic properties, followed by calculation of the binding free energy. The drug-likeness parameters were also calculated, and their values related to absorption, distribution, elimination, and toxicity in the human body were provided for future selection of the best candidates for in vivo testing. It is expected that the results obtained for this group of compounds for the first time will facilitate further investigations into their behavior in terms of transport and distribution, mechanism of binding, pharmacodynamics, and pharmacokinetics.

2. Materials and methods

2.1. Experimental section

2.1.1. Chemical compounds

All chemicals were purchased from major chemical suppliers as high or highest purity grade and utilized without any further purification. Melting points were determined using an Electrothermal 9001 Digital Melting Point apparatus. The chemical structure of the synthesized compounds was confirmed by their spectral data (^{1}H NMR and ^{13}C NMR 1D and 2D spectra in solution, which were recorded using either a Varian 300 V NMR S or a Bruker Avance DMX 400 spectrometer). Chemical shifts σ (ppm) in solutions were referenced to TMS. The purity of the compounds was verified by elemental analyses using the C, H, N Elementary GmbH Vario EL III apparatus. For thin layer chromatography (TLC) prepared plates Merck Kieselgel 60 F_{254} were used (toluene/dioxane/ethanol 6.0/3.2/0.5 or CH_2Cl_2/methanol 99/1 and 99.5/0.5). For column chromatography Merck Silicagel 60, 230–400 mesh ASTM (0.040–0.063 mm) was used. All compounds were prepared following previously reported procedures, and their atom numbering, ^{1}H NMR and ^{13}C NMR spectra are available in the ESI [37,38].

2.1.2. Reagents and sample preparation

All solvents were of analytical grade and used without further purification. Chemicals including KCl, NaCl, HCl, KOH, NaH_2PO_4 and Na_2HPO_4, dipyridamole (DIP) and AGP (catalog number G98885) were purchased from Sigma Aldrich. Doubly distilled Milli-Q water was utilized for sample preparation. Samples for AGP binding studies were prepared in phosphate-buffered saline (PBS) at pH = 7.4. Protein stock solutions were prepared in PBS buffer, and their concentration was calculated based on their UV–vis absorption: $\varepsilon_{280\ nm}$ (AGP) = 24,140 M^{-1} cm^{-1} [40,41]. Stock solutions (c = 1 mM) of the pentamidine derivatives were prepared in water, and their concentrations were determined based on a weight-in-volume basis. In AGP binding experiments, these stocks were diluted with PBS to achieve working solutions (c = 100–200 μM).

2.1.3. pH-potentiometry

pH-Potentiometric measurements were conducted at 25.0 ± 0.1 °C in water within the pH range of 2.0 and 11.5, and at a constant ionic strength of 0.10 M KCl. The titrations were performed in a carbonate-free KOH solution (0.10 M). The exact concentrations of HCl and KOH solutions were determined through pH-potentiometric titrations. A Metrohm 904 Titrando automated titrator equipped with a Metrohm combined electrode (type 6.0258.600) was employed for the pH-potentiometric measurements. The electrode system was calibrated according to the method suggested by Irving et al. [42]. The water ionization constant (pK_w) was determined to be 13.76 ± 0.01, consistent with literature data [43]. The initial sample volume was 10.0 ml, with the ligand concentration ranging from 1.0 to 1.5 mM. Inert gas was passed over the solutions 10 min before and during the titrations. The computer program Hyperquad2013 was used to determine the proton dissociation constants (pK_a) similarly as it was performed in our previous works [44–46].

2.1.4. UV–vis spectrophotometric measurements

UV–vis spectra were recorded using an Agilent Carry 8454 diode array spectrophotometer within the wavelength range of 190 to 1100 nm, with a path length (l) of 0.5 or 1.0 cm. The pH-dependent spectrophotometric titrations were performed over the pH range of 1.0 to 11.6 on samples containing 20 to 50 μM compound at 25.0 ± 0.1 °C and an ionic strength of 0.10 M KCl. The same titrator system was used for the pH-potentiometric titrations. Proton dissociation constants together with the individual molar absorbance spectra were calculated using the computer program HypSpec2014 employing the Newton-Raphson iterative method [44].

2.1.5. Direct experimental determination of lipophilicity

The distribution coefficients (D_{pH}) of the compounds were determined using the shake-flask method in *n*-octanol/buffered aqueous solution at pH = 7.4 (PBS) at 25.0 ± 0.2 °C, following previously described procedures [47]. The ligands were dissolved in *n*-octanol pre-saturated aqueous solution of the buffer at concentrations ranging from 50 to 60 μM. Subsequently, the aqueous samples were mixed with *n*-octanol in a 1:1 volume ratio and stirred for 2 h. Phase separation was aided by centrifugation, after which the UV–vis spectrum of the compound in the aqueous phase was compared to that of the original stock solution. The D_{pH} value of the compounds was calculated according to the following equation:

$$D_{pH} = \frac{Abs_{(stock.sol.)}}{Abs_{(aqueous\ phase\ after\ separation)}} - 1$$

2.1.6. Interaction with α_1-acid glycoprotein – spectrofluorometric measurements

Steady-state fluorescence spectra were recorded using a Fluoromax (Horiba, Jobin Yvon) spectrofluorometer. Samples were measured in 1 × 1 cm cells at 37 °C. Each sample contained 1 μM AGP and was titrated by pentamidines up to 32 ligand-to-protein ratios. The excitation and emission wavelengths were set to 280 nm and 290–450 nm, respectively. The conditional binding constants (K) were calculated using the computer program HypSpec2014 [44], following methodologies described in our previous works [48,49]. Calculations were always based on data obtained from at least two independent measurements. Corrections for self-absorbance and inner filter effect were necessary and were performed according to methodologies outlined in our former works, employing the formula suggested by Lakowicz [48–50].

Fluorescence anisotropy measurements were conducted for the AGP–DIP–pentamidine systems (2 μM: 2 μM: 0–50 μM). The following ligands were tested: **1a**, **3a**, **1b**, **3b$_1$**, **3c** and **3d**. The fluorescence anisotropy signal (I) of DIP was followed at λ_{EX} = 400 nm and λ_{EM} = 500 nm using an automated polarizer set mounted into the steady-state instrument. Emission intensity was measured according to procedures described in our previous work [51]. The G-factor was determined separately (G = 0.94). The FluorEssence v.3.9 software automatically calculated the overall anisotropy(<r>).

2.1.7. Ultrafiltration

Ultrafiltration was applied to separate protein-ligand samples into low and high molecular mass (LMM and HMM) fractions as described in our former work [48]. Membrane filters of 3 kDa cut-off (Millipore,

Amicon Ultra-0.5) were used and ligands **1a**, **3a**, **1b**, **3b$_2$**, **1d** and **3d** were assayed. The samples contained 10 μM AGP and 10 μM pentamidine derivative in PBS (pH = 7.4). The concentration of the non-bound compounds in the LMM fractions was determined by UV–vis spectrophotometry, comparing the recorded spectra to those of reference samples lacking the protein.

2.2. Theoretical calculations

2.2.1. Preparation of pentamidine derivatives and AGP

Thirteen pentamidine derivatives were analyzed in various forms including di-cationic (**1a** – **3a**, **1b** – **3b$_1$**, **2d** and **3d**), tri-cationic (**1c** – **3c**) and tetra-cationic (**3b$_2$** and **1d**) (see Fig. 1) forms in parts of the theoretical studies. The starting conformations of ligands were constructed based on the solid-state structures from diffraction X-ray and ^{13}C CP/MAS NMR data of structurally related compounds using Discovery Studio v.21 interface BIOVIA [52]. Subsequently, the geometries of all compounds were optimized using the density functional theory (DFT) with the B3LYP/6-311G (d,p) hybrid functional, as implemented in Gaussian16 [53]. ESP-atomic partial charges on all atoms were computed using the Breneman model to reproduce the molecular electrostatic potential [54]. The structures were exported into three-dimensional SDF files and introduced into the software ADMET Predictor™ version 11 [55] to calculate the values of molecular descriptors by the independent mathematical models employed in the ADMET programme. The crystal structure of AGP (PDB ID: 3KQ0, resolution of 1.8 Å) was obtained from RCSB PDB (https://www.rcsb.org/pdb). The three-dimensional structure of AGP represents an unglycosylated form, which does not contain any *N*-glycans. The prepare AGP for docking, any heterogeneously bound ligand ((2*R*)-2,3-dihydroxypropyl acetate and chloride ion) and crystallographic water molecules were removed. Additionally, hydrogen atoms were added and merged with nonpolar hydrogen atoms.

2.2.2. Calculation of drug-likeness-related properties for pentamidine derivatives

The molecular structures of tested pentamidine derivatives were used as input to the mathematical models implemented in the ADMET Predictor™ program to generate estimates for each of the drug-likeness properties. In this study, Lipinski's rule of five was checked and the following descriptors were calculated: topological polar surface area (TPSA), logD distribution coefficient (at pH = 7.4), proton dissociation constants (pK_a), solubility (S_w), the volume of distribution (V_d), Madina-Darby renal cell apparent permeability (MDCK), effective permeability (P_{eff}), absorbed fraction (%F_a) and bioavailable fraction (%F_b), blood-brain BBB filter, blood-brain barrier partition coefficient (logBB), percentage of unbound drug to plasma protein (%Unbnd) and blood-to-plasma concentration ratio (RBP). Furthermore, the likelihood of interactions with potential membrane transporters was assessed using five models to classify the mode of action (substrate or inhibition): P-glycoprotein (P-gp), the breast cancer resistance protein (BCRP), the hepatic organic anion transporting polypeptides (OATP1B1 and OATP1B3), the hepatic organic cation transporters (OCT1 and OCT2), and the bile salt export pump (BSEP). The selected toxicity profile was characterized by the maximum recommended therapeutic dose (MRTD), the affinity towards hERG-encoded potassium channels (hERGfilter and hERGpIC$_{50}$) joined with cardiac toxicity, and the levels of five hepatic enzymes (alkaline phosphatase (AlkPhos), γ-glutamyl transferase (GGT), serum glutamate oxaloacetate transaminase (SGOT), serum glutamate pyruvate transaminase (SGPT), and lactate dehydrogenase (LDH)) as hepatotoxicity indicators.

2.2.3. Initial system configurations: molecular docking

Molecular docking is an important computational procedure performed to find out the exact binding site on a protein that fits geometrically and energetically with a ligand. In this study, the CDOCKER protocol, implemented in Discovery Studio v.21 and relying on the CHARMm force field [56], was employed for molecular docking analysis. The active site was defined within a radius of 20 Å around the ligand present in the 3KQ0 crystal. The ligands were allowed to interact with residues in the defined binding site spheres to generate 30 conformations. The results were obtained based on the CDOCKER interaction energies [57], which represent the energy of the nonbonded interactions between the protein and the ligand. Finally, the complex conformation with the lowest energy was extracted and the molecular dynamics simulations (MD) were performed by Discovery Studio v.21 to assess the reliability of the docking results. This step helps to validate the stability and dynamics of the protein-ligand complex over time, providing further insights into the binding interactions.

2.2.4. Interaction with AGP: molecular dynamics simulations

MD simulations of ligand-AGP complexes were performed in a solution to better reflect the experimental systems and intermolecular interactions that play a key role in their stability. During MD simulation, the systems were placed in a dodecahedron water box solvated by TIP3P water model and neutralized by the addition of Na^+ ions. The energy minimization was carried out using the steepest descent method for 5000 steps followed by 5000 steps of the conjugate gradient to relax bad steric collisions between atoms. The system was heated up to 300 K for 50 ps and then equilibrated for 100 ps at 1 bar in the NPT ensemble. Temperature and pressure controls were controlled by the Berendsen thermostat. Finally, MD simulation was performed for 100 ns. The particle mesh Ewald (PME) algorithm was used to analyses long-range electrostatic interactions. The trajectories from the MD simulations were saved for every 50 ps intervals for analyses of root mean square deviation (RMSD), root mean square fluctuation (RMSF) and radius of gyration (R_g) as well as the protein-ligand contacts.

To further delineate the AGP-ligand complex, time-based binding free energy (ΔG_{bind}) calculations were performed. The Molecular Mechanics/Poisson-Boltzmann Surface Area (MM/PBSA) method was employed for this purpose and was conducted after the MD simulations [58]. The obtained ΔG_{bind} considers the protein fluctuations and the ligand conformations, thus ensuring the correct location of the ligand within the binding pocket. The binding free energy AGP-ligand complex in a solvent system is stated as $\Delta G_{bind} = G_{complex} - G_{AGP} - G_{ligand}$, where $G_{complex}$ refers to the total free energy of the AGP-ligand complex and G_{AGP} and G_{ligand} indicate the separated protein AGP and ligand in the solvent. All energy is averaged over the MD trajectories.

3. Results and discussion

3.1. Prediction of drug-likeness and toxicity for pentamidine derivatives

In the preliminary test, the compliance of the analyzed compounds to Lipinski's rule of five and the calculation of the topological polar surface area (TPSA) was checked. Lipinski's rule of five is commonly used in drug design and development to predict the oral bioavailability of potential lead molecules or drugs. In contrast, the TPSA is a useful parameter for predicting the transport properties of drugs. It quantifies the sum of surface areas occupied by polar atoms (usually oxygen, nitrogen, and attached hydrogen atoms) in a molecule. The results are summarized in Table S1 in the Supplementary material. As can be seen, all the selected pentamidine derivatives have molecular weights (MWt) in the 355–462 g/mol, which falls within the recommended limit of <500 g/mol, except for compound **3a** due to the presence of a bromine atom substituent at the 2-position in the aromatic rings. Generally, drug molecules with a low MWt < 500 g/mol are easily absorbed, distributed, and transported compared to heavy molecules. MWt is an important aspect of the therapeutic effect of a drug; if it increases sufficiently, the effect of the drug is affected [59]. The number of atoms that can be engaged in intermolecular hydrogen bonding is above or exactly the acceptable range. This parameter is significant as it influences the

Table 1
Prediction of absorption parameters and the fraction absorbed (%F_a) and fraction bioavailable (%F_b) in selected species at a specific dose for pentamidine derivatives in various models.

Compound	S_w	P_{eff}	MDCK	%F_a	%F_b
	Expected values for good drug candidates				
	(≥ 0.010 mg/ml)	(≥ 0.5 cm/s·10^4)	(≥ 30 cm/s·10^7)	Dose 10.0 mg	
1a	6.74	0.49	216.30	74.67	62.00
2a	0.66	0.88	340.52	97.63	82.77
3a	2.66	0.67	272.03	92.68	81.00
1b	13.82	0.43	175.70	66.85	53.10
2b	1.92	0.75	279.94	91.57	80.08
3b$_1$	3.49	0.25	107.85	53.91	48.77
3b$_2$	4.47	0.39	60.17	59.25	51.14
1c	6.11	0.68	282.96	81.04	72.97
2c	5.32	0.71	311.52	82.96	73.62
3c	9.63	0.52	250.77	73.16	62.86
1d	3.85	0.26	62.55	44.87	38.18
2d	1.53	0.30	125.84	58.57	54.69
3d	0.70	0.71	578.19	84.98	75.86

compound's ability to interact with target proteins or receptors, thereby affecting its pharmacological activity. The values of the logarithm of the distribution coefficient (logD) at pH = 7.4, which estimate the lipophilicity of ionisable substances, range from −1.72 to 1.51 and are consistent with experimental values. Negative logD values lead to the conclusion that these compounds would be more distributed in the aqueous phase than in lipophilic biomolecules. The TPSA values of all compounds were calculated and found to be within the range of 106 to 224 Å^2. The O- and N- atoms concentrated as polar fragments are included. Compounds **2a** and **3a** exhibited the highest degree of lipophilicity, indicating good lipid solubility, and facilitating interaction with the cell membranes. Conversely, compounds **1a**, **1b**, **3b$_1$**, **3b$_2$**, **1d** and **2d** demonstrated TPSA values above 140 Å^2, suggesting their potential to penetrate hydrophilic environments.

The analysis included parameters related to absorption and transport, such as water solubility (S_w), effective permeability (P_{eff}), apparent permeability (MDCK), fraction absorbed (%F_a) and fraction bioavailable (%F_b), and affinities for five major drug uptake and efflux transporters located on the tubular membrane of hepatocytes: P-glycoprotein (P-gp), breast cancer resistance protein (BCRP), bile salt export pump (BSEP), organic anion transporting polypeptide 1B (OATP1B1), and renal organic cation transporter 2 (OCT2). The values of these parameters are shown in Tables 1 and 2.

The aqueous solubility (S_w) of all tested pentamidine derivatives (remember that these are the following hydrochlorides: di-cationic (**1a** – **3a**, **1b** – **3b$_1$**, **2d** and **3d**), tri-cationic (**1c** – **3c**) and tetra-cationic (**3b$_2$** and **1d**)), is notably high, and are within the range of 0.66–13.82 mg/ml. The compound with the best solubility is 1,5-*bis*(4-amidino-2,6-dimethoxyphenoxy)-3-oxapentane dihydrochloride (**1b**) (13.82 mg/ml). The permeability of the human jejunum (P_{eff}), which reflects the passive transport velocity in cm/s across the epithelial barrier in the human jejunum, is predicted for tested *bis*-amidines in the region of 0.25–0.71 × 10^{-4} cm/s, indicating their average permeability of the jejunum. MDCK as a parameter to predict apparent membrane permeability properties for Madin-Darby Canine Kidney cells ranged from 60.17 to 578.19 × 10^{-7} cm/s. The lowest values of both parameters are predicted for 1,5-*bis*(4-amidino-2-aminophenoxy)-3-oxapentane tetrahydrochloride (**3b$_2$**) and 1,5-*bis*[(4-amidino-2-aminophenyl)amino]-3-oxapentane tetrahydrochloride (**1d**), indicating that the introduction of additional amino groups on the aromatic rings reduces jejunal permeability and apparent membrane permeability. Then, using the ACAT™ model implemented in the ADMET Predictor program, the precent absorbed (%F_a) and oral bioavailability (%F_b) were estimated for pentamidine derivatives based on their molecular structure. The dosage form considered was an immediate-release tablet (IR Tablet), with a dose set at 10 mg/kg. The values of the parameters are presented in Table 1 and Fig. S1 in Supplementary material. In the oral bioavailability dataset, the molecules with bioavailability (%F) values ≥70 % were considered to have high bioavailability, while those with <70 % were categorized as low bioavailability [60]. According to results presented in Table 1 and Fig. S1, all compounds except **1b**, **3b$_1$**, **3b$_2$**, **1d** and **2d**, were predicted to have %F_a and %F_b values above 70 %. This suggests favorable absorption and oral bioavailability for most of the tested pentamidine derivatives. The best bioavailability at a dose of 10 mg was demonstrated in three dihydrochlorides: **2a** and **2b** (with four methyl groups at the *ortho* positions in benzene rings), and **3a** (with bromine and methoxy substituents), 82.8 %, 80.1 % and 81.0 %, respectively. The analysis of the probability of affinity for transporters belonging to the ATP-binding cassette (ABC) gene family reveals that the tested *bis*-amidines may be substrates for P-gp, which can pump toxins or drugs out of cells [61] but cannot be inhibitors (see Table 2). Additionally, all compounds have been identified as substrates of breast cancer resistance protein (BCRP), indicating a potential risk for drug resistance. *Bis*-amidines lack the potential to inhibit organic anion transport polypeptide 1B1 (OATP1B1) and 1B3 (OATP1B3) and have been predicted not to be inhibitors of bile salt export pumps (BSEP). Our study shows that the tested compounds acted as substrates and inhibitors of both OCT transporters, except for **1a**, **3b$_1$** and **3b$_2$**, which were identified as substrates for OCT1. It should be noted that OCTs refer to one of the most abundant liver transporters and OCTs are considered polyspecific membrane transporters that function by mediating the hepatic uptake of hydrophilic compounds that are small and positively charged. Inhibition of OCT2 may interfere with renal secretion and alter drug accumulation in the kidney, causing nephrotoxicity.

The prediction of tissue distribution of a drug is another important

Table 2
Mode of action (inhibition/substrate) of selected transporters models for pentamidine derivative.

Compound	P-gp substrate	BCRP substrate	BSEP inhibitor	BSEP_IC_{50} ≤60 μM	OATP1B1 and OATP1B3 inhibitor	OCT1 substrate/inhibitor	OCT2 substrate/inhibitor
1a	Yes	Yes	No	38.1	No	Sub	Sub/Inh
2a	Yes	No	No	16.6	No	Sub/Inh	Sub/Inh
3a	Yes	No	No	21.5	No	Sub/Inh	Sub/Inh
1b	Yes	Yes	No	45.4	No	Sub/Inh	Sub/Inh
2b	Yes	Yes	No	15.5	No	Sub/Inh	Sub/Inh
3b$_1$	Yes	Yes	No	12.5	No	Sub	Sub/Inh
3b$_2$	Yes	Yes	No	10.8	No	Sub	Sub/Inh
1c	Yes	Yes	No	11.1	No	Sub/Inh	Sub/Inh
2c	Yes	Yes	No	12.8	No	Sub/Inh	Sub/Inh
3c	Yes	Yes	No	31.2	No	Sub/Inh	Sub/Inh
1d	Yes	Yes	No	10.7	No	Sub/Inh	Sub/Inh
2d	Yes	Yes	No	11.8	No	Sub/Inh	Sub/Inh
3d	Yes	Yes	No	13.2	No	Sub/Inh	Sub/Inh

Table 3
Prediction of the distribution for pentamidine derivatives in different models.

Compound	V_d	%Unbnd	RBP	BBB filter	logBB
	Expected values				
	(≤ 3.7 l/kg)	(>10 %)	(<1)	(high/low)	
1a	3.23	16.03	0.86	low	−0.19
2a	4.92	9.42	1.03	low	0.05
3a	4.26	8.74	0.90	low	0.09
1b	2.76	24.86	0.87	low	−0.28
2b	4.19	14.10	1.04	low	−0.05
$3b_1$	2.17	9.97	1.04	low	−0.001
$3b_2$	4.56	27.84	1.29	low	−0.45
1c	5.45	21.16	1.12	low	0.20
2c	5.53	19.41	1.07	low	0.20
3c	4.55	18.43	0.97	low	0.04
1d	5.99	28.76	1.28	low	−0.40
2d	4.67	5.57	1.15	low	0.16
3d	7.71	11.18	1.06	low	0.28

consideration in assessing the potential of molecules as therapeutic agents. Molecular descriptors such as V_d, %Unbnd, RBP, BBB_filter and logBB have been proven to be useful in modelling distribution (see Table 3). The volume of distribution (V_d) is a pharmacokinetic parameter that can indicate the theoretical volume required to achieve a drug concentration equal to a specified plasma concentration. The V_d of all tested *bis*-amidines ranges from 2.17 to 7.71 l/kg, suggesting that they may not be uniformly distributed to all tissues in the body. Compounds with a V_d of <3.7 l/kg are found predominantly in plasma, but ten of the tested compounds have values higher than 4 l/kg and are expected to be distributed throughout whole blood (**2a**, **3a**, **2b**, **$3b_2$**, **1c** – **3c** and **1d** – **3d**). On the other hand, binding to HSA may increase the biological half-life of the drug. Two parameters characterize these properties: the percentage of drug unbound to protein within blood plasma (%Unbnd) and the concentration of the drug in whole blood compared to plasma (RBP).

For the analyzed pentamidine derivates, the values of %Unbnd range from 5.57 to 28.76 %, and the values of RBP range from 0.87 to 1.29 (see Table 3 and Fig. S2 in Supplementary material). As shown in Fig. S2, only compounds **1a**, **1b** and **3c**, which include 2,6-dimethoxy- or 2-methoxy- substituents, avoid regions of both high RBP partitioning and extensive plasma protein binding. This suggests that these compounds are free of RBP metabolism and can efficiently reach the therapeutic target, which is an ideal characteristic of an effective drug. Compounds **2a**, **2b** – **$3b_2$**, **1d** – **3d**, **1c** and **2c** fall within a region suggesting that they could interact with other blood components (for example – hemoglobin, carbonic anhydrase, or the cell membrane) [62–64]. Another important property of a potential drug is its ability to cross the blood-brain barrier (BBB), which should be high for CNS therapeutics and low for other applications. The BBB_filter parameter indicated low permeability, and the values of logBB's range from −0.45 to 0.28, indicating high-to-moderate permeation for all tested compounds. The logBB values for 1,5-*bis*[(4-amidinophenyl)-*N*-methyl-amino]pentane dihydrochloride (**3d**) was found to be close to 0.3, suggesting that this type of substitution increases the potential for BBB penetration of drugs.

The study additionally paid special attention to pK_a values, since the biopharmaceutical profile of the compound depends directly on the dissociation constants of its acid and base groups. Most drugs contain multiple ionization sites, and although only one site is generally ionized in the pH range of interest, understanding which site is ionized at physiological pH is crucial, especially when charge localization is needed to study ligand-protein interactions. The ionization of one group can influences the deprotonation (pK_a) of the next group; therefore, it is critical to correctly predict the ionization pattern of a multiprotic compound, a task that is challenging not only for prediction methods but also for experimental methods, which generally cannot identify which ionizable site is associated with the observed pK_a. Furthermore,

Table 4
Proton dissociation constants (pK_a) and the standard deviations (±SD) of selected pentamidine derivatives determined by pH-potentiometry and/or UV–vis spectrophotometry {$I = 0.1$ M KCl; 25 °C} and prediction of the negative logarithm of proton dissociation constant (pK_a).

Compound	pK_a (anilinium) UV–vis	pK_a (ammonium) pH-potentiometry	pK_a predicted
$3b_2$	2.39 ± 0.01	–	2.75
1c	–	7.00 ± 0.01[a]	6.69
2c	–	7.27 ± 0.01	6.66
3c	–	6.99 ± 0.01	6.57
1d	2.49 ± 0.01	–	4.29
2d	< 1.0	–	−0.06
3d	1.58 ± 0.01	–	4.31

[a] pK_a = 7.04 ± 0.01 determined by UV–vis titration.

experimental methods like pH-potentiometry and UV–vis spectrophotometry are suitable to determine macro constants, although the predicted pK_a values of all compounds fall in the range of −0.06 to 16.21 (Table 4 and Table S1 in Supplementary material). Fig. S3 in the Supplementary material illustrates the possible forms of amidine, aniline-like and amine functional groups involved in proton dissociation processes in pentamidines. The observed macrostates for pentamidine derivatives are complex mathematical functions of the relevant microstates. They are assignable only to transitions between the various net charge states of the pentamidine molecule, i.e., H_3M^{+3}, H_2M^{+2} and HM^{+}. For di-cationic compounds **1a** – **3a**, **1b** and **2b**, the protonation of the -NH_2 in amidine substituents is proposed at a very high pH (pH > 16.0). In turn, in compound **$3b_1$** which presents two additional nitro groups, protonation occurred at both moieties (-NH_2 and -NO_2) at a slightly lower pK_a = 15.2, but still does not have relevance from a biological point of view. The protonation of the aniline-like functional groups in **1d** – **3d** and **$3b_2$** is predicted to occur within a lower pH range (pH < 4.3). The pK_a value of aliphatic ammonium groups in trihydrochloride pentamidine derivatives **1c** – **3c** ranges between 6.00 and 7.00, consistent with the obtained experimental data (see Table 4).

To be considered a potential drug candidate in clinical trials, a compound should possess an acceptable pharmacokinetic profile and a high safety margin, minimizing probability of toxicity and potent adverse effects. The toxicity profile of all pentamidines was evaluated using several predictors, including human maximum tolerated dose, cardiotoxicity, and hepatotoxicity (see Table 5).

The threshold of the maximum recommended therapeutic dose (MRDT) is 3.16 (mg/kg/day). All compounds tested (except **$3b_1$** and **2d** with 2-nitro groups) have MRDT values below 3.16 (mg/kg/day), indicating active compounds but with the potential for side effects. The calculated estimation of the likelihood of the hERG potassium channel inhibition (hERGfilter) and the pIC_{50} as a measure of affinity for hERG K^+ channel (hERGpIC_{50}) is promising for all compounds – they can be classified as non-cardiotoxic. Only one compound 1,5-*bis*(4-amidino-2-bromo-6-methoxyphenoxy)pentane dihydrochloride (**3a**), can be classified as cardiotoxic. In the liver damage test, most of the tested pentamidine derivates are rated as ńon-toxic'. Levels of LDH, SGOT, and SGPT are elevated only for **2a, 3a, 2b, $3b_1$** and **1d** indicating some hepatic problems. The cytotoxicity of these compounds was studied experimentally in our earlier work [38] with other groups of pentamidine derivates that can be classified as non-toxic or much less toxic than the parent compound pentamidine, which may explain the observed data.

3.2. Proton dissociation processes and lipophilicity of the pentamidine derivatives

The proton dissociation processes were also experimentally investigated for the derivatives containing aliphatic amine (**1c** – **3c**) and aniline-like functions (**1d** – **3d**, **$3b_2$**) in detail (see Chart S1 in

Table 5
Predicted toxicity parameters for pentamidine derivatives.

Compound	MRDT	hERG filter	hERG pIC_{50}	AlkPhos	GGT	LDH	SGOT	SGPT
	Expected values							
	(>3.16 mg/kg/day)	(Yes/No)	(>5.5)					
1a	Below 3.16	Yes	5.3	NT	T	NT	T	T
2a	Below 3.16	Yes	5.3	NT	T	T	T	T
3a	Below 3.16	Yes	5.5	NT	T	T	T	T
1b	Below 3.16	Yes	5.2	NT	T	NT	T	T
2b	Below 3.16	Yes	5.2	NT	T	T	T	T
$3b_1$	Above 3.16	No	4.4	NT	T	T	T	T
$3b_2$	Below 3.16	Yes	5.2	NT	NT	NT	T	T
1c	Below 3.16	Yes	5.2	NT	T	NT	T	T
2c	Below 3.16	Yes	5.3	NT	T	NT	T	T
3c	Below 3.16	Yes	5.1	NT	T	NT	T	T
1d	Below 3.16	Yes	5.2	NT	NT	T	T	T
2d	Above 3.16	No	4.3	NT	NT	NT	T	T
3d	Below 3.16	No	5.3	NT	NT	NT	T	NT

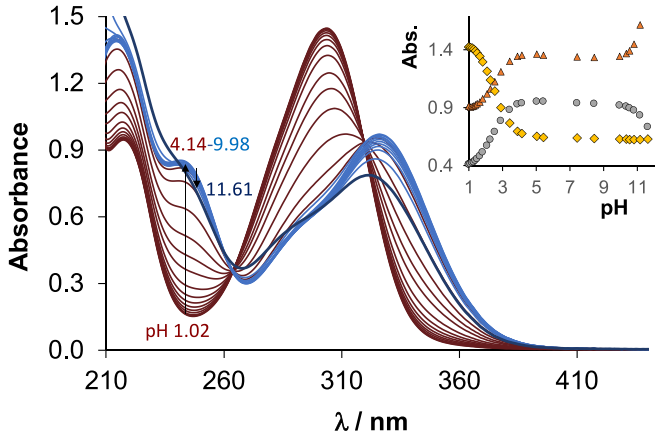

Fig. 2. Absorption spectra of **1d** recorded in the pH = 1.02–11.61, the inserted figure shows the absorbance changes at 207 nm (▲) 300 nm (♦) and 330 nm (●), {c = 77 μM; ℓ = 0.5 cm; I = 0.1 M (KCl), t = 25 °C}.

Supplementary material for terminology of the respective groups). Proton dissociation constants (pK_a) were determined by pH-potentiometry and UV–vis spectroscopic titrations at 0.1 M KCl ionic strength and 25 °C and are collected in Table 4. All title compounds possess two amidine functional groups (see Charts S1 in Supplementary material). According to the pH-potentiometric titrations, these groups remain protonated at pH < 10.0 for **1c** – **3c**, **1d** – **3d**, **$3b_2$** and **2a**. The predicted pK_a values in Fig. S3 confirm the experimental observation. Due to the relatively high uncertainty of the determined amidinium pK_a values, they are not listed here. Similar high pK_a values are expected for the amidinium groups found in the other five derivatives, therefore they were not subjected to pH-potentiometric titrations. The protonation of the aniline-like functions in **1d** – **3d** and **$3b_2$** typically occurs in the pH range pH < 3.0 according to the pH-potentiometric titration curves. As Fig. 2 shows for **1d** the deprotonation of the anilinium function results in bathochromic shift of the UV–vis absorption spectra between pH = 1 and 4 (see also Figs. S4 and S5 in Supplementary material).

The well-defined isosbestic points at 264 nm and 320 nm suggest that one deprotonation process takes place, namely only one of the two aniline groups is involved, and the other group cannot be protonated at pH ≥ 1.0. Proton dissociation constants and individual UV–vis spectra of the different protonation forms were calculated using HypSpec software and are presented in Table 4 and Fig. S5 in Supplementary material [44]. The deprotonation of the amidinium moiety is accompanied by fewer characteristic changes above pH = 10, and the absence of isosbestic points between pH = 10 and 11.6 refers to overlapping deprotonation processes of the two amidinium moieties, therefore no constant could be calculated. Interestingly, no pK_a could be determined for the aniline-like group in **2d** in the acidic pH range. This is most probably due to the electron-withdrawing effect of the nitro substituent introduced in the ortho position to the -NHR moiety. The pK_a of the aliphatic ammonium groups in **1c** – **3c** varies between pH = 6.99 and 7.27 (see Table 4). These latter three compounds are partly +3 and + 2 charged at pH = 7.4; the distribution is as follows: H_3L^{3+}: 28 % (**1c** and **3c**) and 43 % (**2c**). The other ligands (**1a** – **3a**, **1b**, **2b**, **$3b_1$**, **$3b_2$**, **1d** – **3d**) are exclusively present in +2 charged form, protonated on the two amidinium moieties. Experimental and predicted values are in good agreement for the ammonium groups in **1c**, **2c** and **3c,** as well as the anilinium group in **$3b_2$** and **2d**. Experimental constants for **1d** and **3d** are lower by 1.8 and 2.7 pH units, respectively, compared to the predicted macro constants in Fig. S3.

The lipophilicity of the compounds was assessed through *n*-octanol/water partition experiments, and distribution coefficients ($D_{7.4}$) were determined at pH = 7.4 and 25 °C, as listed in Table S1 in Supplementary material (see representative UV–vis spectra in Fig. S6 in Supplementary material). According to the obtained data, most of the studied compounds are hydrophilic, with **2a** and **3a** being the only exceptions, which prefer the nonpolar solvent over the aqueous buffer. The compounds **1b**, **1c**, **3c** and **1d** are extremely hydrophilic, with only a distribution limit ($\log D_{7.4} < 1.7$) estimable. Some correlations can be concluded on the basis of $\log D_{7.4}$ values: (i) the complete MeO → Me exchange (in **1a**/**2a** and **1b**/**2b**) increases the lipophilicity of the molecule, (ii) also the partial MeO → Br exchange results in similar effect (**1a**/**3a**), (iii) the introduction of a third ether group into the chain decreases the lipophilicity (**1a**/**1b** and **2a**/**2b**) and (iv) in general chains with three heteroatoms are more hydrophilic than those containing only two heteroatoms. The presence of an -NH_2 group instead of -NO_2 on the aromatic ring has no unequivocal influence on the *n*-octanol/water distribution. Notably, the determined distribution values apply to most of the ligands in a wide pH range (pH = 3–10), while the distribution of **1c** – **3c** may change considerably with pH due to the presence of the protonatable amine group. It is worth comparing predicted and experimental $\log D_{7.4}$ values (Table S1 in the Supplementary material). The predicted lipophilicity of the amino-derivatives **1c** - **3c** are overestimated compared to the experimental values (e.g. -0.34 (calc.) vs. -1.31 (exp.) for **2c**). This is most probably due to the underestimation of the pK_a values and consequently, the underestimation of the +3 charged species presents at pH 7.4 for these molecules. Predictions for the nitro derivatives (**$3b_1$** and **2d**), as well as for the methoxy ligands (**1a** and **1b**) and **2a**, show higher lipophilicity by about 0.8–1.6 order of magnitude compared to the experimentally determined ones. This observation confirms that it is worthwhile to determine simple physico-chemical parameters experimentally as well, if possible.

Table 6
Fluorescence and UV–vis absorption parameters of the studied molecules, excitation, (λ_{EX}), emission (λ_{EM}) and absorption (λ_{Abs}) maxima, together with the molar absorption coefficients (ε). {pH 7.4 (PBS); 25 °C}.

Compound	$\lambda_{EX(max)}$[a] (nm)	$\lambda_{EM(max)}$[a] (nm)	Rel. intensity[b] (%)	$\lambda_{Abs(max)}$[a] (ε)[c] (nm ($M^{-1} \times cm^{-1}$))
1a	268	395	50	268 (15100)
2a	253	358	100	250 (21900)
3a	260, 290[d]	380	3.5	258 (14100) 290 (6290)[e]
1b	268	394	51	268 (13400)
2b	258	358	100	250 (20500)
$3b_1$	–	–	0	241 (34500) 323 (4200)
$3b_2$	260, 303[d]	468	1.1	228 (35700) 265 (11900) 307 (6800)
1c[f]	257	333	63	259 (26900)
2c	257	333	78	258 (24900)
3c	263, 290[d]	387	18	263 (19500) 293 (12900)
1d	323	500	1.8	241 (21400) 325 (24000)
2d	–	–	0	267 (31600) 295 (30700) 420 (9200)
3d	270, 330[d]	395	7.1	328 (27200)

[a] Standard deviation of the wavelength maxima is ±2 nm.
[b] Calculated from the peak intensities at λ_{EX}(max) and λ_{EX}(max).
[c] Standard deviation of ε values was ±50 $M^{-1} \times cm^{-1}$.
[d] The underlined wavelength was used for relative intensity calculation.
[e] Not a well-defined band but a shoulder.
[f] Fluorescence and absorbance parameters of the H_3L^{3+} form: λ_{EX}(max) = 257 nm; λ_{EM}(max) = 333 nm; I_{rel} = 111 %; λ(max) = 256 nm ε = 27,000 $M^{-1} \times cm^{-1}$, and the H_2L^{2+} form: λ_{EX}(max) = 263 nm; λ_{EM}(max) = 333 nm; I_{rel} = 10 %; λ(max) = 261 nm ε = 27,000 $M^{-1} \times cm^{-1}$.

3.3. Characterizing fluorescence properties

The studied pentamidines are fluorescent, except for the two nitro-derivatives, **$3b_1$** and **2d**. The important fluorescence parameters of the compounds, together with their molar absorptivities registered at pH = 7.4 (PBS) and 25 °C, are listed in Table 6. The wavelength of the excitation and absorption maxima are generally very similar, with the only exception being **3d**, where the molecule could also be excited at 270 nm (see Fig. S7 in Supplementary material), where the predominant form has no absorbance band. The introduction of extra substituents on the aromatic rings fundamentally influences the wavelength (energy) of the emitted light. Electron-donating groups with positive mesomeric effects result in a red-shifted emission band. The extent of the shift corresponds to the strength of the mesomeric effect of the respective groups, with NH_2 > MeO (see e.g. **$3b_2$** and **3c** in Table 6) [65]. The exchange of the O-linker to the NR-linker results in the same effect (cf. **1c** and **3d**). Additionally, the number of introduced substituents matters, e.g., **1a** with two MeO-substituents per aromatic ring, which displays a more red-shifted emission than **3c** (one MeO per ring). The presence of a bromine with a negative inductive effect in **3a** counterbalances the mesomeric effect of MeO in some extent. The methyl substituents in **2a** and **2b** results in only moderate red shift compared to the non-substituted derivatives (**1c** and **2c**) due to the positive inductive effect of this group. Regarding the intensity, it can be concluded that the non-substituted derivatives (**2a**, **1c** and **2c**) are the most emissive molecules. It must be noted that protonation of the aliphatic amine in **1c** and **2c** results in higher fluorescence intensity (see footnote for **1c** in Table 6). The introduction of bromine (**3a**) and NH_2 or NR_2 substituents (**3d**, **$3b_2$** and **1d**) greatly reduces the fluorescence efficacy, while the presence of a nitro substituent completely quenches the fluorescence of the molecules (**$3b_1$** and **2d**). The fluorescence lifetime of the emissive compounds is rather short (τ < 0.2 ns); therefore, it could not be determined with the available instrumentation.

Although the analysis of these properties may seem like lexical material, they provide important information for possible fluorescence microscopic applications. They are also useful when, for example, direct monitoring of cellular uptake of molecules is planned or when the possibility of interference with conventional staining methods needs to be assessed. These molecules exhibit relatively low fluorescence, and the derivatives with emission capacity in the visible region are even less fluorescent, therefore, no significant alterations in microscopic imaging are expected.

3.4. Binding to α_1-acid glycoprotein, fluorescence, and ultrafiltration studies

In our recent study, we highlighted that human serum albumin (HSA) does not exhibit a preference for binding related pentamidine ligands [39]. Knowing that HSA prefers to bind negatively charged and neutral small molecules in its three hydrophobic binding sites (Sudlow's sites I and II and a third site in subdomain IB), our interest turned to investigation the binding of these molecules with AGP. AGP prefers to bind molecules with basic functional group(s) in its central hydrophobic cavity. The present molecules possess a + 2 charge at pH 7.4 due to the two amidine groups; furthermore, **1c**, **2c** and **3c** are partly +3 charged at this pH. This raises the possibility of a prominent role for AGP in the transport of these drugs.

First, fluorometric quenching experiments were carried out with the AGP and the pentamidine derivatives. In Fig. 3a, a gradual decrease in AGP fluorescence is depicted upon the addition of **3a**. It can be observed in Fig. 3b, that the quenching is not complete although saturation could be attained by the addition of ca. 30 equiv. ligand. The lack of complete

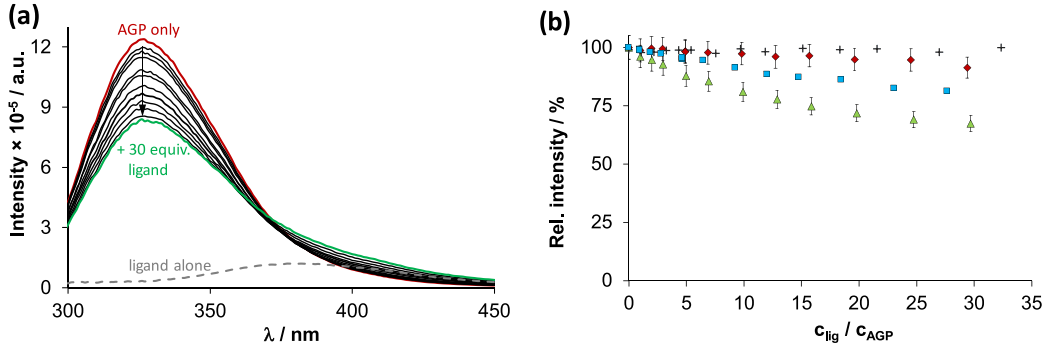

Fig. 3. (a) Fluorescence emission spectra of AGP in the absence and presence of **3a** and (b) the quenching curves at λ_{EM} = 325 nm for **3a** (▲), **3d** (■), **1a** (◆) and **$3b_2$** (+) error bars denote the standard deviation of the measured intensities for **3a** and **1a** determined from three titrations, 2–2 titration were done with **3d** and **$3b_2$**, the relative deviations did not exceed 6 % {c_{AGP} = 1.0 μM; c_{lig} = 0–33 μM; $c_{lig\ alone}$ = 30 μM (a); λ_{EX} = 280 nm; pH = 7.4 (PBS); t = 37 °C}.

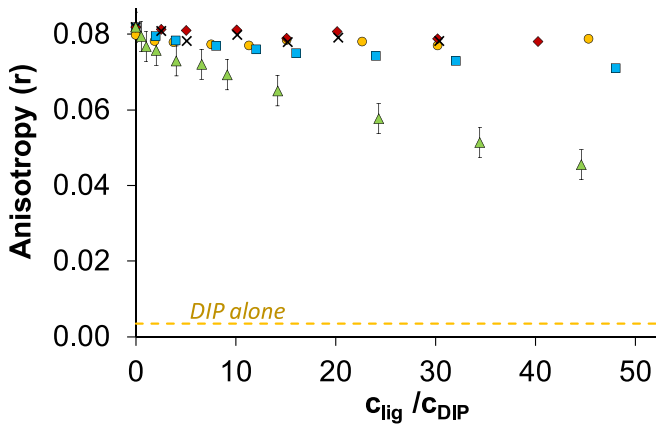

Fig. 4. Fluorescence anisotropy (r) of the AGP – DIP system in the absence and presence of various pentamidine derivatives: **3a** (▲), **3d** (■), **1a** (◆), and **1b** (×); anisotropy signal of free DIP (yellow dashed line, $r = 3.0 \times 10^{-3} \pm 8 \times 10^{-4}$) is indicated as well. Error bars denote the standard deviation of r for **3a** {c_{AGP} = 2.0 μM; c_{DIP} = 2.0 μM; λ_{EX} = 400 nm; λ_{EM} = 500 nm; pH = 7.4 (PBS), 37 °C}.

quenching is normal since AGP contains three highly fluorescent Trp moieties from which only Trp-25 and Trp-122 residues lie inside and next to the central binding cavity, respectively [66]. Only two compounds, **3a** and **3d** could considerably quench the fluorescence of AGP, while **1a** showed weak quenching. The other ten derivatives displayed no quenching upon the addition of 30 equiv. of ligand. Interestingly, the emission bands of **3a** and **3d** were not sensitive to protein binding. Conditional binding constants (K) were calculated using HypSpec software for the AGP–**3a** ($\log K = 4.7 \pm 0.1$) and AGP–**3d** ($\log K = 4.4 \pm 0.1$) systems [44]. The software allowed us to handle the strongly overlapping spectra of AGP and the ligands (further examples of quenching titrations can be found in Fig. S8 in Supplementary material). The quenching assay strongly suggests that most of the ligands do not bind into the central cavity of AGP, since they did not considerably quench the fluorescence of the protein. However, it should be noted that AGP contains three fluorescent Trp amino acids, not all of them situated at the central binding cavity, so quenching studies carry a degree of uncertainty. Therefore, further fluorescence anisotropy and ultrafiltration studies were carried out.

The AGP binding was further investigated through dipyridamole (DIP) displacement studies. DIP binds to AGP in the central site with high affinity and is highly fluorescent in the visible range. Displacement of DIP can be excellently monitored via fluorescence anisotropy measurements, as direct steady-state measurement is not applicable due to the emission intensity of DIP being insensitive to protein binding [51,67]. Fluorescence anisotropy experiments indicate well the size and shape of a fluorophore by measuring the polarized emission of a solution [50]. As depicted in Fig. 4, AGP-bound DIP possesses higher anisotropy due to the slower rotational diffusion of the protein, and the anisotropy decreases when DIP is liberated from AGP. A significant decrease in anisotropy was observed only for **3a**, and a slight reduction was detected in the case of **3d**. This agrees well, with the results of the quenching experiments. The results of DIP displacement experiments suggest that these two derivatives bind in the hydrophobic cavity.

The ultrafiltration technique could only be used for a few ligands, as most of them adhered to the filter surface. In the case of **3a**, **3d**, **1a** and **1b,** adhesion to the filter was >70 %. For **1d** and **3b$_2$**, adhesion was 44–45 %, considering this, only 2 % and 6 % AGP binding could be observed at 1:1 M ratio, respectively (see representative UV–vis spectra in Fig. S9 in the Supplementary material). Overall, **3a** and **3d** show moderate binding affinity towards AGP. The compound **3a** is the most lipophilic ($\log D_{7.4} = +0.65$, Table S1 in Supplementary material) among the studied ligands. However, there is no clear trend between lipophilicity and binding affinity since **3d** is less lipophilic than **2a** (cf. $\log D_{7.4} = -0.24$ and + 0.34), the former binds to AGP while the latter showed no protein binding.

3.5. *Characterization of the binding site pentamidine derivatives by molecular docking*

In parallel with experimental techniques, the binding of pentamidine derivatives was investigated theoretically by docking ligands to the obtained AGP crystal structure to elucidate the location of molecule binding on AGP, the key amino acid residues involved, and the type of

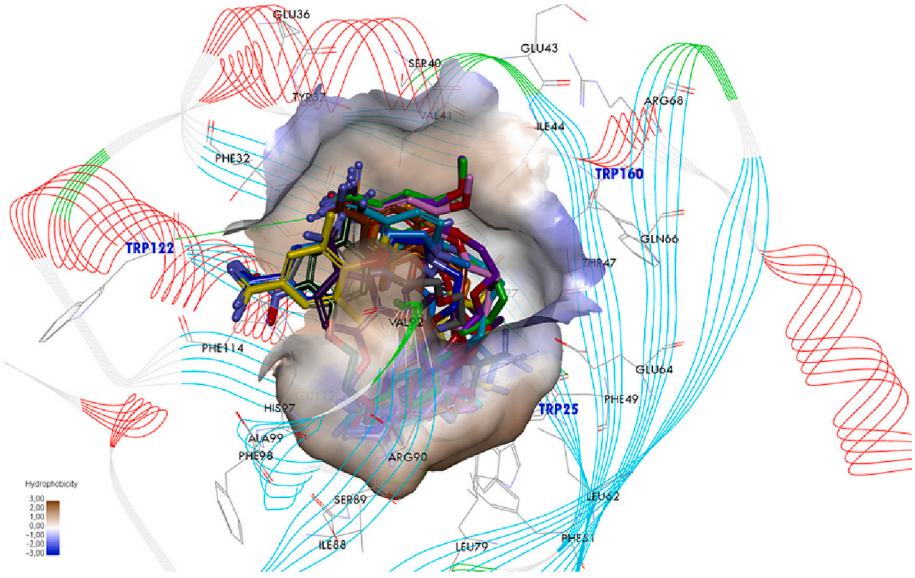

Fig. 5. Close-up view of an active site of the AGP structure after molecular docking. Surface hydrophobicity was depicted by the shaded colors: brown - the hydrophobic and blue – the hydrophilic regions. Predicted superposition of compounds: **1a** (C atoms shown as green), **1b** (C atoms shown as magenta), **1c** (C atoms shown as blue), **1d** (C atoms shown as red), **2a** (C atoms shown as yellow), **2b** (C atoms shown as brown), **2c** (C atoms shown as dark blue), **2d** (C atoms shown as grey), **3a** (C atoms shown as pink), **3b$_1$** (C atoms shown as dark green), **3b$_2$** (C atoms shown as orange), **3c** (C atoms shown as violet) and **3d** (C atoms shown as turquoise).

Table 7
Theoretical and experimental free energies of binding to AGP, and theoretical average distance of ligand to Trp-25 and Trp-122 for pentamidine derivatives **1a**, **3a** and **3d**.

Compounds	ΔG_{bind} (kcal/mol)	ΔG_{exp}[a] (kcal/mol)	r_{Trp-25} (Å)	$r_{Trp-122}$ (Å)
1a	−1.75	–	11.22	12.79
3a	−13.15	−6.67	10.11	7.46
3d	−11.30	−6.24	11.14	10.58

[a] $\Delta G_{exp} = -2.303$ RT log$K$.

interaction force. The 3KQ0 crystal structure of AGP shows a β-barrel like structure comprising eight antiparallel β-strands connected by four loops and three α-helices flanking around the β-barrel. The ligand binding pocket is located within the β-barrel motif. The binding pocket of AGP contains three lobes (I-III). Lobe I constitute a major non-polar sub-compartment of the binding cavity and thus favors the binding of hydrophobic ligands. The residues that form lobe I are Tyr-27, Phe-51, Leu-62, Leu-79, Ile-88, Ala-99, Leu-101, Leu-102, Tyr-110, Leu-112 and Tyr-127. Lobe I is flanked by much smaller lobes II and III. Lobe II is lined by Phe-49, Glu-64, Gln-66, Ile-73 and Arg-90, while lobe III is lined by Phe-32, Ala-113, Phe-114, Asp-115 and Ser-125 residues. Molecular docking was conducted within lobe I as the most probably pocket for pentamidine derivatives. The most favorable thirteen conformations of **1a** – **3a**, **1b** – **3b$_2$**, **1c** – **3c** and **1d** – **3d** with the lowest docking energy were found in 30 independent runs (Fig. 5).

In this case, docking identified an unambiguous, bent binding mode, and the molecules fit into a well-defined binding site but exhibited diverse positions and interactions with residues of AGP in the respective pentamidine derivative groups. The tested compounds were held in the binding site by a combination of hydrogen bonds, and hydrophobic and van der Waals interactions with their surroundings. Compounds **1a**, **1b**, **1d**, **2b**, **3a**, **3b$_2$** and **3d** are predicted to cluster more centrally in the binding cavity of AGP than **1c**, **2a**, **2c**, **2d**, **3b$_1$** and **3c**, which are accommodated at the entrance of AGP pocket (see Fig. S10 in Supplementary material). Further analysis of the binding site revealed that the benzamidine groups in **1a**, **1b**, **1d**, **2b**, **3a**, **3b$_2$** and **3d** primarily interact with Phe-32, Tyr-37, Val-41, Ile-88, Arg-90 and His-97, whereas in compounds **1c**, **2a**, **2c** and **2d**, interactions are formed with Tyr-37, Arg-90, Val-92, His-97, Tyr-127 and Asn-121. Positions **3b$_1$** and **3c** allow the formation of interactions with an extended network of hydrophobic contacts with the aromatic residues (Ser-30, Tyr-37 and Val-92). It can be observed that seven pentamidine derivatives (**1a**, **1b**, **1d**, **2b**, **3a**, **3b$_2$** and **3d**) were close to Trp-25 and Trp-122 residues in the range of 8.5–12.52 Å and away from Trp-160 residues. In contrast, the other compounds (**1c**, **2a**, **2c**, **2d**, **3b$_1$** and **3c**) are situated at a distance from Trp residues above 13 Å without making direct contact with any of the three Trp residues. In the 3KQ0 structure, the accessibility of Trp-25 in the cavity is obstructed by the side chain of Tyr-110, hence close contact with the ligand is generally hindered. Among all the pentamidine derivatives analyzed, compounds **1a**, **3a** and **3d** were closest to the Trp-25 and Trp-122 residues, where the molecular distance between the benzamidine ring and the core benzene ring in tryptophan residues was for **1a** (Trp-25 (10.55 Å) and Trp-122 (12.52 Å)), **3a** (Trp-25 (10.54 Å) and Trp-122 (8.99 Å)) and **3d** (Trp-25 (10.71 Å) and Trp-122 (9.96 Å)), and shown distinct differences in their binding capacity.

This confirms that the formation of these three complexes easily leads to the quenching of two residues, which is cross-checked with the fluorescence spectroscopy results. Hence, in further studies, molecular dynamics simulation and binding free energy calculations were performed for the three complexes (AGP-**1a**, AGP-**3a** and AGP-**3d**) to better understand the various interactions between the ligand and the active site of AGP and to rationalize the obtained experimental results.

3.6. Interactions with *1a, 3a and 3d* in the AGP

The intermolecular interactions at the active site of AGP were analyzed for the averaged structures of the complexes (AGP-**1a**, AGP-**3a**, and AGP-**3d**) obtained from MD simulations. The theoretical values of binding free energy were calculated and are shown in Table 7 with experimental values obtained using Gibbs isotherms and log$K$ values ($\Delta G_{exp} = -2.303$ RT log$K$). From the most favorable conformations pentamidines given in Fig. 6 and the corresponding energy parameters (Table 7), it was observed that **3a** where bromine and methoxy substituents at amidine groups are present, binds more favorably to the hydrophobic cavity in AGP with $\Delta G_{bind} = -13.15$ kcal/mol (corresponding to log$K = 4.7 \pm 0.1$) in comparison with **3d** ($\Delta G_{bind} = -11.30$ kcal/mol, log$K = 4.4 \pm 0.1$). In contrast, for compound **1a**, the binding free energy value calculated by the MM/PBSA method was −1.75 kcal/mol, which, as indicated by the fluorescence experiment, resulted in negligible fluorescence intensity for this compound. The calculated binding free energies and the experimentally obtained values maintain a consistent trend, with a maximum difference of approximately ~6.48 kcal/mol. A possible explanation may be that the X-ray structure of the protein from crystals differs from that of the aqueous system used in this study. The structures of the three complexes AGP-**1a**, AGP-**3a**, and AGP-**3d** and detailed interactions are shown in Fig. 6.

Complex AGP-**1a** which is characterized by the lowest binding free energy is stabilized by much less intermolecular interactions than complexes AGP-**3a** and AGP-**3d**. One can observe the week hydrogen bonds with the residues Tyr-37 (3.46 Å), Arg-90 (2.98 Å) and His-97 (2.94 Å), the electrostatic interactions of the -NH_2^+ group with Glu-36 (5.39 Å), and the hydrophobic interactions with residues Val-41, Val-92, Leu-79, Leu-112 and Phe-114. Noteworthy, compound **1a** is unable to form stability with the protein by unfavorable donor-donor interaction with Arg-90. The two complexes AGP-**3a** and AGP-**3d**, characterized by high binding free energies, are stabilized mainly by hydrogen bonding and hydrophobic interactions. It is predicted that compound **3a** to be placed in the AGP active site in a bent conformation, while compound **3d** is placed in a U-shaped conformation, which may account for its smaller affinity compared to **3a**. The predicted location of both 4-amidino-2-bromo-6-methoxyphenoxy (**3a**) and 4-amidinophenyl-*N*-methylamino (**3d**) substituents allowed for the many interactions with important residues to lobes I, II and III of AGP. One amidine group of compound **3a** creates the strong hydrogen bond with residues His-97 (2.28 Å), Phe-114 (2.95 Å), Asn-117 (2.86 Å) and Asn-121 (2.65 Å), whereas compound **3d** forms the hydrogen bonds with the residues Ile-88 (3.05 Å) and His-97 (3.05 Å). Apart from typical interactions, the amidine groups facilitate the electrostatic interactions with the AGP. It can also be observed that in compound **3a**, the bromine atom and methoxy group at the benzene rings located deep in the binding pocket form hydrophobic interactions with five residues Phe-32 (3.96 Å), Glu-64 (3.35 Å), Val-92 (3.69 Å), Phe-114 (4.18 Å) and Tyr-127 (3.62 Å), whereas the aliphatic linker type of -O-chain-O- forms hydrophobic contacts with Val-41 (4.41 Å) and Ile-44 (5.19 Å) residues. In addition, it can be observed that key hydrophobic residues such as Tyr-27 (5.24 Å) and Leu-62 (5.33 Å) in lobe I, and Phe-32 (3.63 Å) and Phe-114 (3.41 Å) in lobe III of AGP interact with the phenyl ring. Meanwhile, the folded conformation of compound **3d** allows for favorable interactions of the *N*-methyl groups in the aliphatic linker with hydrophobic residues from lobe I (Leu-62 (4.25 Å) and Leu-79 (4.35 Å)), and Tyr-27 (4.09 Å), Val-41 (4.80 Å), and Ile-44 (5.07 Å).

Compounds **3a** and **3d**, which exhibit the highest affinity, are closer to Trp-25 and Trp-122 compared to compounds **1a** (see Table 5). Based on our findings, the heteroatoms (-NCH_3) in the aliphatic linker and the addition of a —Br atom and a methoxy substituent at the C-2 and C-6 positions to the benzene rings of the *bis*-amidine are essential for strong interactions with the binding site of AGP.

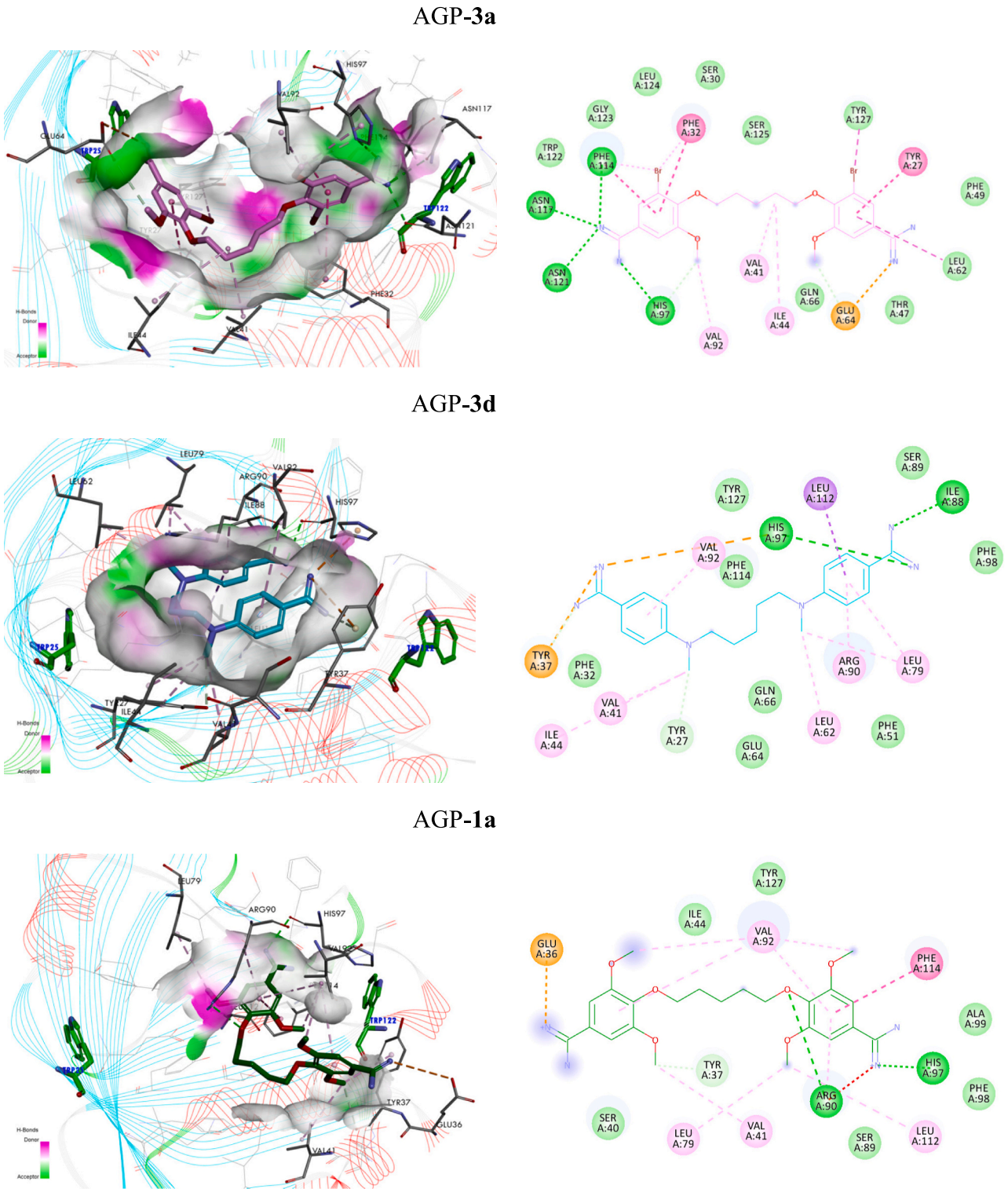

Fig. 6. Locations of pentamidines on AGP after in silico simulations and two-dimensional interaction diagram between compounds **1a**, **3a** and **3d** with key amino acid residues in AGP and relationship between acceptors and donors.

*3.7. Stiffness of AGP-**3a**/**3d** complexes observed from MD simulation data*

To investigate the binding affinity and secondary structural changes induced by *bis*-amidines, the MD simulation trajectories of free AGP and the AGP-ligand complex were performed and compared. To measure the structural properties in this study, we used root mean square deviation (RMSD), radius of gyration (R_g), root mean square fluctuation (RMSF), and qualitative stability, stiffness, and conformational changes of AGP were compared during the time of simulation.

Based on the agreement of experimental and computational evidence, the conformation of the two complexes (AGP-**3a** and AGP-**3d**) with the lowest free binding energy was chosen. The binding modes of the compounds were analyzed in terms of RMSD deviations of the ligands throughout the simulation time from the starting input structure. The RMSD values of the atoms in the free AGP and the complexed one

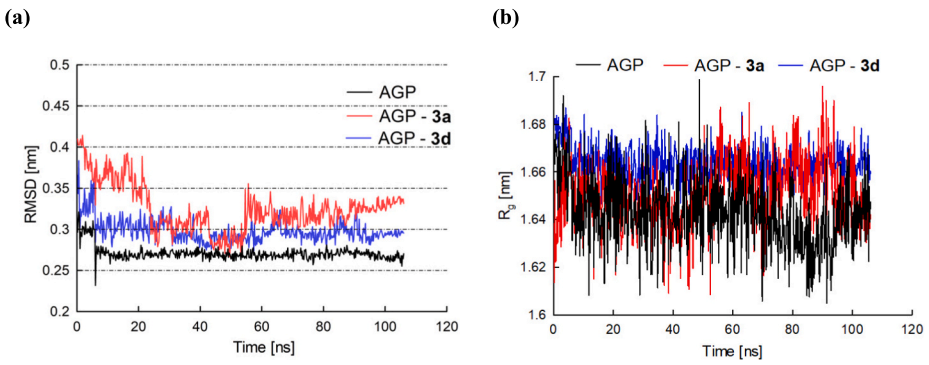

Fig. 7. Molecular dynamics simulation of AGP-**3a**/**3d** complexes throughout 100 ns. (**a**) RMSD values for AGP main chain with and without compounds **3a** and **3d**; (**b**) The R_g value of AGP with and without compounds **3a** and **3d**.

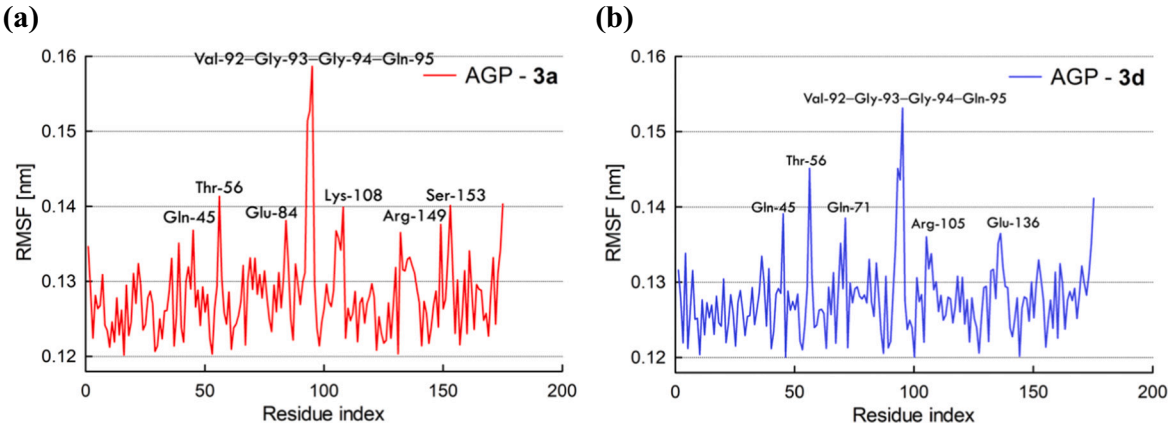

Fig. 8. Root mean squared fluctuation over residues numbers for AGP-**3a** (**a**) and AGP-**3d** (**b**).

were plotted in the range of 0–100 ns, as shown in Fig. 7a. The analysis indicated that the RMSD of free AGP reaches equilibrium and oscillates around an average value of approximately 0.3 nm after 10 ns of simulation time, while the complexes (AGP-**3a** and AGP-**3d)** initially exhibited fluctuations and stabilized after 60 ns of simulation trajectories, with the RMSD values of around 0.3 nm. It has been observed from the RMSD plot of the AGP backbone that there were no significant conformational changes in the protein structure during MD simulation time. On the other hand, in the complexes with AGP, the ligands (**3a** and **3d**) did not induce any notable conformational changes in the AGP structure. They exhibited stability in their bound conformations inside the protein's active site pocket. Then, the time evolution of the radius of gyration (R_g) value of free AGP and AGP-**3a**/**3d** complexes was estimated, and the outcomes were charted in Fig. 7b. The R_g provides a direct measure of the compactness of the protein structure. The outcomes indicated an increase in R_g values for the AGP-**3d** system compared to the AGP system. Based on the assumption that the lower the R_g value, the more compact the structure of the AGP protein, we can conclude that binding with **3d** contributes to the loosening of the AGP structure. In the AGP-**3a** complex, R_g values were stabilized during the simulation up to 50 ns and the last 10 ns. The R_g values of both AGP free and AGP-**3a** complex were about ~1.65 nm. These results indicate that the radius of the gyration value is compatible with compound **3a** complexation with respect to free AGP. Therefore, it was concluded that the structure of the AGP in the presence of **3a** is stably folded during MD simulation. Thus, based on the RMSD and R_g values obtained from our MD simulation data, it was concluded that AGP shows little structural change when combined with compounds **3a** and **3d**.

To investigate the change in flexibility of each residue during the binding of pentamidines **3a** and **3d** to AGP, the RMSF value of each residue, which represents the position deviation from the reference position during the entire simulation period, was calculated and is shown in Fig. 8 and Fig. S11 in Supplementary material.

The results revealed that the RMSF values for each residue in the **3a**-AGP and **3d**-AGP complexes differed from those observed for free AGP (see Fig.S11 in Supplementary material). The RMSF values of residues Gln-45, Thr-56, Glu-84, Glu-71, Gly-93, Gly-94, Glu-95, Arg-105, Lys-108, Glu-136, Arg-149, and Ser-153 in AGP increased significantly upon binding to pentamidine derivatives **3a** and **3d** compared to free AGP. This suggests that the fluctuation of these residues increased due to the binding of pentamidines. In contrast, the RMSF values of other residues declined, indicating that the movement of these residues was greatly restrained. This observation suggests that the change in the synchronous fluorescence spectra of the Trp residues may have been induced by the ligand, potentially indicating a conformational change of the AGP rather than a direct interaction with the ligand.

4. Conclusion

To our knowledge, this is the first study to identify the interaction between α_1-acid glycoprotein and *bis*-benzamidines as pentamidine derivatives. We have applied spectroscopy techniques and computer simulations of molecular docking and molecular dynamics analyses to reveal the detailed interaction mechanism by which *bis*-benzamidines bind to plasma protein. The thirteen pentamidine derivatives investigated that showed high activity against *Pneumocystis carinii,* represent an interesting group of compounds with better drug-likeness properties than pentamidine alone. The best bioavailability was shown by three compounds such as **2a** and **2b** (with four methyl groups at the ortho positions in the benzene rings), and **3a** (with bromine and methoxy

substituents). The studied compounds undergo transitions between various net charge states of the pentamidine molecule, i.e., H_3M^{+3}, H_2M^{+2} and HM^{+}, at physiological pH (pH = 7.4). Investigations of the affinity of pentamidine derivatives for AGP by fluorescence quenching spectroscopy showed significant binding of pentamidines **3a** and **3d**, while the other derivatives showed weak or no binding, suggesting a specific role for AGP as a carrier molecule for *bis*-benzamidines. For these compounds, the experimental data were in good agreement with the calculated free energies of binding obtained through docking methods and MD simulations of the ligand in the binding pocket. Compounds **3a** and **3d** emerge as potential candidates for recognition by this protein. Hydrogen bonding, electrostatic, and hydrophobic interactions played a significant role in stabilizing the complexes between AGP and pentamidine derivatives. The research has provided accurate and quantifiable data on the binding mechanism of pentamidine derivatives with drug carrier protein of AGP, contributing to an understanding of its effect on serum protein function during distribution in the bloodstream.

CRediT authorship contribution statement

Teresa Żołek: Writing – review & editing, Writing – original draft, Validation, Methodology, Formal analysis, Data curation, Conceptualization. **Orsolya Dömötör:** Writing – review & editing, Methodology, Investigation, Formal analysis. **Jerzy Żabiński:** Investigation.

Declaration of competing interest

The authors declare that they have no known competing financial interests or personal relationships that could have appeared to influence the work reported in this paper.

Acknowledgement

O.D. gratefully acknowledges the financial support from TKP-2021-EGA-32 project of the Development and Innovation Office-NKFIA (Hungary).

Appendix A. Supplementary data

Supplementary data to this article can be found online at https://doi.org/10.1016/j.ijbiomac.2024.131405.

References

[1] M.T. Rehman, A.U. Khan, Understanding the interaction between human serum albumin and anti-bacterial/ anti-cancer compounds, Curr. Pharm. Des. 21 (14) (2015) 1785–1799.
[2] Z.H. Israili, P.G. Dayton, Human alpha-1-glycoprotein and its interactions with drugs, Drug Metab. Rev. 33 (2) (2001) 161–235.
[3] D.N. Bailey, J.R. Briggs, The binding of selected therapeutic drugs to human serum alpha-1 acid glycoprotein and to human serum albumin in vitro, Ther. Drug Monit. 26 (1) (2004) 40–43.
[4] S.A. Smith, N.J. Waters, Pharmacokinetic and pharmacodynamic considerations for drugs binding to alpha-1-acid glycoprotein, Pharm. Res. 36 (2) (2018) 30.
[5] T. Fournier, N.N. Medjoubi, D. Porquet, Alpha-1-acid glycoprotein, Biochim. Biophys. Acta 1482 (1–2) (2000) 157–171.
[6] Z. Huang, T. Ung, Effect of alpha-1-acid glycoprotein binding on pharmacokinetics and pharmacodynamics, Curr. Drug Metab. 14 (2) (2013) 226–238.
[7] C.B. Eap, J.F. Fischer, P. Baumann, Variations in relative concentrations of variants of human alpha 1-acid glycoprotein after acute-phase conditions, Clin. Chim. Acta 203 (2–3) (1991) 379–385.
[8] M. Otagiri, A molecular functional study on the interactions of drugs with plasma proteins, Drug Metab. Pharmacokinet. 20 (5) (2005) 309–323.
[9] J.R. Albani, Progesterone binding to the tryptophan residues of human alpha1-acid glycoprotein, Carbohydr. Res. 341 (15) (2006) 2557–2564.
[10] H. Shiono, A. Shibukawa, Y. Kuroda, T. Nakagawa, Effect of sialic acid residues of human alpha 1-acid glycoprotein on stereoselectivity in basic drug-protein binding, Chirality 9 (3) (1997) 291–296.
[11] M.A. Azad, J.X. Huang, M.A. Cooper, K.D. Roberts, P.E. Thompson, R.L. Nation, J. Li, T. Velkov, Structure-activity relationships for the binding of polymyxins with human alpha-1-acid glycoprotein, Biochem. Pharmacol. 84 (3) (2012) 278–291.
[12] S. Karthikeyan, G. Bharanidharan, S. Ragavan, S. Kandasamy, S. Chinnathambi, K. Udayakumar, R. Mangaiyarkarasi, A. Sundaramoorthy, P. Aruna, S. Ganesan, Comparative binding analysis of N-acetylneuraminic acid in bovine serum albumin and human alpha-1 acid glycoprotein, J. Chem. Inf. Model. 59 (1) (2019) 326–338.
[13] K. Hanada, Lipophilicity influences drug binding to alpha1-acid glycoprotein F1/S variants but not to the a variant, Drugs R D 17 (3) (2017) 475–480.
[14] M.R. Ajmal, S. Nusrat, P. Alam, N. Zaidi, M.V. Khan, M. Zaman, Y.E. Shahein, M. H. Mahmoud, G. Badr, R.H. Khan, Interaction of anticancer drug clofarabine with human serum albumin and human alpha-1 acid glycoprotein. Spectroscopic and molecular docking approach, J. Pharm. Biomed. Anal. 135 (2017) 106–115.
[15] D.P. Yeggoni, A. Rachamallu, M. Kallubai, R. Subramanyam, Cytotoxicity and comparative binding mechanism of piperine with human serum albumin and alpha-1-acid glycoprotein, J. Biomol. Struct. Dyn. 33 (6) (2015) 1336–1351.
[16] S. Alsford, J.M. Kelly, N. Baker, D. Horn, Genetic dissection of drug resistance in trypanosomes, Parasitology 140 (12) (2013) 1478–1491.
[17] P.G. Bray, M.P. Barrett, S.A. Ward, H.P. de Koning, Pentamidine uptake and resistance in pathogenic protozoa: past, present and future, Trends Parasitol. 19 (5) (2003) 232–239.
[18] N. Bruni, B. Stella, L. Giraudo, C. Della Pepa, D. Gastaldi, F. Dosio, Nanostructured delivery systems with improved leishmanicidal activity: a critical review, Int. J. Nanomedicine 12 (2017) 5289–5311.
[19] A. Clark, T. Hemmelgarn, L. Danziger-Isakov, A. Teusink, Intravenous pentamidine for Pneumocystis carinii/jiroveci pneumonia prophylaxis in pediatric transplant patients, Pediatr. Transplant. 19 (3) (2015) 326–331.
[20] L. Liu, F. Wang, Y. Tong, L.F. Li, Y. Liu, W.Q. Gao, Pentamidine inhibits prostate cancer progression via selectively inducing mitochondrial DNA depletion and dysfunction, Cell Prolif. 53 (1) (2020) e12718.
[21] M.D. Libman, M.A. Miller, G.K. Richards, Antistaphylococcal activity of pentamidine, Antimicrob. Agents Chemother. 34 (9) (1990) 1795–1796.
[22] D. Maciejewska, J. Zabinski, P. Kazmierczak, K. Wojciuk, M. Kruszewski, H. Kruszewska, In vitro screening of pentamidine analogs against bacterial and fungal strains, Bioorg. Med. Chem. Lett. 24 (13) (2014) 2918–2923.
[23] K.J. Edwards, T.C. Jenkins, S. Neidle, Crystal structure of a pentamidine-oligonucleotide complex: implications for DNA-binding properties, Biochemistry 31 (31) (1992) 7104–7109.
[24] T. Sun, Y. Zhang, Pentamidine binds to tRNA through non-specific hydrophobic interactions and inhibits aminoacylation and translation, Nucleic Acids Res. 36 (5) (2008) 1654–1664.
[25] N. Paracini, L.A. Clifton, M.W.A. Skoda, J.H. Lakey, Liquid crystalline bacterial outer membranes are critical for antibiotic susceptibility, Proc. Natl. Acad. Sci. U. S. A. 115 (32) (2018) E7587–E7594.
[26] M.K. Pathak, D. Dhawan, D.J. Lindner, E.C. Borden, C. Farver, T. Yi, Pentamidine is an inhibitor of PRL phosphatases with anticancer activity, Mol. Cancer Ther. 1 (14) (2002) 1255–1264.
[27] C.M. Stahl-Bayliss, C.M. Kalman, O.L. Laskin, Pentamidine-induced hypoglycemia in patients with the acquired immune deficiency syndrome, Clin. Pharmacol. Ther. 39 (3) (1986) 271–275.
[28] M.T. Cushion, P.D. Walzer, A. Ashbaugh, S. Rebholz, R. Brubaker, J.J. Vanden Eynde, A. Mayence, T.L. Huang, In vitro selection and in vivo efficacy of piperazine- and alkanediamide-linked bisbenzamidines against Pneumocystis pneumonia in mice, Antimicrob. Agents Chemother. 50 (7) (2006) 2337–2343.
[29] J.E. Hall, J.E. Kerrigan, K. Ramachandran, B.C. Bender, J.P. Stanko, S.K. Jones, D. A. Patrick, R.R. Tidwell, Anti-pneumocystis activities of aromatic diamidoxime prodrugs, Antimicrob. Agents Chemother. 42 (3) (1998) 666–674.
[30] I. Jarak, M. Marjanovic, I. Piantanida, M. Kralj, G. Karminski-Zamola, Novel pentamidine derivatives: synthesis, anti-tumor properties and polynucleotide-binding activities, Eur. J. Med. Chem. 46 (7) (2011) 2807–2815.
[31] M.P. Barrett, D.W. Boykin, R. Brun, R.R. Tidwell, Human African trypanosomiasis: pharmacological re-engagement with a neglected disease, Br. J. Pharmacol. 152 (8) (2007) 1155–1171.
[32] S. Neidle, L.R. Kelland, J.O. Trent, I.J. Simpson, D.W. Boykin, A. Kumar, W. D. Wilson, Cytotoxicity of bis(phenylamidinium)furan alkyl derivatives in human tumour cell lines: relation to DNA minor groove binding, Bioorg. Med. Chem. Lett. 7 (11) (1997) 1403–1408.
[33] A. Lansiaux, F. Tanious, Z. Mishal, L. Dassonneville, A. Kumar, C.E. Stephens, Q. Hu, W.D. Wilson, D.W. Boykin, C. Bailly, Distribution of furamidine analogues in tumor cells: targeting of the nucleus or mitochondria depending on the amidine substitution, Cancer Res. 62 (24) (2002) 7219–7229.
[34] C.M. Nunn, T.C. Jenkins, S. Neidle, Crystal structure of d(CGCGAATTCGCG) complexed with propamidine, a short-chain homologue of the drug pentamidine, Biochemistry 32 (50) (1993) 13838–13843.
[35] M.L. Berger, D. Maciejewska, J.J. Vanden Eynde, M. Mottamal, J. Zabinski, P. Kazmierczak, M. Rezler, I. Jarak, I. Piantanida, G. Karminski-Zamola, A. Mayence, P. Rebernik, A. Kumar, M.A. Ismail, D.W. Boykin, T.L. Huang, Pentamidine analogs as inhibitors of [(3)H]MK-801 and [(3)H]ifenprodil binding to rat brain NMDA receptors, Bioorg. Med. Chem. 23 (15) (2015) 4489–4500.
[36] I.O. Donkor, S.K. Jones, R.R. Tidwell, Pentamidine congeners 1: synthesis of cis- and trans-butamidine analogues as anti-pneumocystis carinii pneumonia agents, Bioorg. Med. Chem. Lett. 3 (6) (1993) 1137–1140.
[37] D. Maciejewska, J. Zabinski, P. Kazmierczak, M. Rezler, B. Krassowska-Swiebocka, M.S. Collins, M.T. Cushion, Analogs of pentamidine as potential anti-Pneumocystis chemotherapeutics, Eur. J. Med. Chem. 48 (2012) 164–173.
[38] D. Maciejewska, J. Zabinski, M. Rezler, P. Kazmierczak, M.S. Collins, L. Ficker, M. T. Cushion, Development of highly active anti-Pneumocystis bisbenzamidines: insight into the influence of selected substituents on the in vitro activity, Medchemcomm 8 (10) (2017) 2003–2011.

[39] T. Zolek, O. Domotor, M. Rezler, E.A. Enyedy, D. Maciejewska, Deposition of pentamidine analogues in the human body - spectroscopic and computational approaches, Eur. J. Pharm. Sci. 161 (2021) 105779.
[40] M.F. AlAjmi, M.T. Rehman, R.A. Khan, M.A. Khan, G. Muteeb, M.S. Khan, O. M. Noman, A. Alsalme, A. Hussain, Understanding the interaction between alpha-1-acid glycoprotein (AGP) and potential Cu/Zn metallo-drugs of benzimidazole derived organic motifs: a multi-spectroscopic and molecular docking study, Spectrochim. Acta A Mol. Biomol. Spectrosc. 225 (2020) 117457.
[41] F. Zsila, Y. Iwao, The drug binding site of human alpha1-acid glycoprotein: insight from induced circular dichroism and electronic absorption spectra, Biochim. Biophys. Acta 1770 (5) (2007) 797–809.
[42] H.M. Irving, M.G. Miles, L.D. Pettit, A study of some problems in determining the stoicheiometric proton dissociation constants of complexes by potentiometric titrations using a glass electrode, Anal. Chim. Acta 38 (1967) 475–488.
[43] SCQuery, The IUPAC Stability Constants Database, Academic Software, Version 5.5, Royal Society of Chemistry, London, UK, 1993.
[44] P. Gans, A. Sabatini, A. Vacca, Investigation of equilibria in solution. Determination of equilibrium constants with the HYPERQUAD suite of programs, Talanta 43 (10) (1996) 1739–1753.
[45] J.P. Meszaros, V.F.S. Pape, G. Szakacs, G. Nemeti, M. Denes, T. Holczbauer, N. V. May, E.A. Enyedy, Half-sandwich organometallic Ru and Rh complexes of (N,N) donor compounds: effect of ligand methylation on solution speciation and anticancer activity, Dalton Trans. 50 (23) (2021) 8218–8231.
[46] O. Domotor, S. Aicher, M. Schmidlehner, M.S. Novak, A. Roller, M.A. Jakupec, W. Kandioller, C.G. Hartinger, B.K. Keppler, E.A. Enyedy, Antitumor pentamethylcyclopentadienyl rhodium complexes of maltol and allomaltol: synthesis, solution speciation and bioactivity, J. Inorg. Biochem. 134 (2014) 57–65.
[47] E.A. Enyedy, D. Hollender, T. Kiss, Lipophilicity of kinetically labile metal complexes through the example of antidiabetic Zn(II) and VO(IV) compounds, J. Pharm. Biomed. Anal. 54 (5) (2011) 1073–1081.
[48] O. Domotor, C.G. Hartinger, A.K. Bytzek, T. Kiss, B.K. Keppler, E.A. Enyedy, Characterization of the binding sites of the anticancer ruthenium(III) complexes KP1019 and KP1339 on human serum albumin via competition studies, J. Biol. Inorg. Chem. 18 (1) (2013) 9–17.
[49] E.A. Enyedy, O. Domotor, K. Bali, A. Hetenyi, T. Tuccinardi, B.K. Keppler, Interaction of the anticancer gallium(III) complexes of 8-hydroxyquinoline and maltol with human serum proteins, J. Biol. Inorg. Chem. 20 (1) (2015) 77–88.
[50] J.R. Lakowicz, Principles of Fluorescence Spectroscopy, 3rd ed., Springer, New York, 2006.
[51] O. Domotor, E.A. Enyedy, Evaluation of in vitro distribution and plasma protein binding of selected antiviral drugs (Favipiravir, Molnupiravir and Imatinib) against SARS-CoV-2, Int. J. Mol. Sci. 24 (3) (2023).
[52] D.S. BIOVIA, Discovery Studio, [Version 21], Dassault Systèmes, San Diego, 2021.
[53] M.J. Frisch, G.W. Trucks, H.B. Schlegel, G.E. Scuseria, M.A. Robb, J.R. Cheeseman, G. Scalmani, V. Barone, G.A. Petersson, H. Nakatsuji, X. Li, M. Caricato, A. V. Marenich, J. Bloino, B.G. Janesko, R. Gomperts, B. Mennucci, H.P. Hratchian, J. V. Ortiz, A.F. Izmaylov, J.L. Sonnenberg, D. Williams-Young, F. Ding, F. Lipparini, F. Egidi, J. Goings, B. Peng, A. Petrone, T. Henderson, D. Ranasinghe, V. G. Zakrzewski, J. Gao, N. Rega, G. Zheng, W. Liang, M. Hada, M. Ehara, K. Toyota, R. Fukuda, J. Hasegawa, M. Ishida, T. Nakajima, Y. Honda, O. Kitao, H. Nakai, T. Vreven, K. Throssell, J.A. Montgomery Jr., J.E. Peralta, F. Ogliaro, M. J. Bearpark, J.J. Heyd, E.N. Brothers, K.N. Kudin, V.N. Staroverov, T.A. Keith, R. Kobayashi, J. Normand, K. Raghavachari, A.P. Rendell, J.C. Burant, S.S. Iyengar, J. Tomasi, M. Cossi, J.M. Millam, M. Klene, C. Adamo, R. Cammi, J.W. Ochterski, R.L. Martin, K. Morokuma, O. Farkas, J.B. Foresman, D.J. Fox, Gaussian 16, Gaussian, Inc., Wallingford CT, 2016.
[54] C.M. Breneman, K.B. Wiberg, Determining atom-centered monopoles from molecular electrostatic potentials - the need for high sampling density in Formamide conformational-analysis, J. Comput. Chem. 11 (3) (1990) 361–373.
[55] I. ADMET Predictor v. 10.4.05. Lancaster: Simulations Plus.
[56] B.R. Brooks, R.E. Bruccoleri, B.D. Olafson, D.J. States, S. Swaminathan, M. Karplus, Charmm - a program for macromolecular energy, minimization, and dynamics calculations, J. Comput. Chem. 4 (2) (1983) 187–217.
[57] M.K. Abdel-Hamid, A. McCluskey, In silico docking, molecular dynamics and binding energy insights into the bolinaquinone-clathrin terminal domain binding site, Molecules 19 (5) (2014) 6609–6622.
[58] P.A. Kollman, I. Massova, C. Reyes, B. Kuhn, S. Huo, L. Chong, M. Lee, T. Lee, Y. Duan, W. Wang, O. Donini, P. Cieplak, J. Srinivasan, D.A. Case, T. E. Cheatham 3rd, Calculating structures and free energies of complex molecules: combining molecular mechanics and continuum models, Acc. Chem. Res. 33 (12) (2000) 889–897.
[59] C.A. Lipinski, A.G. Reaume, Phenotypic screening of low molecular weight compounds is rich ground for repurposed, on-target drugs, Front. Pharmacol. 13 (2022) 917968.
[60] T.L. Moda, C.A. Montanari, A.D. Andricopulo, Hologram QSAR model for the prediction of human oral bioavailability, Bioorg. Med. Chem. 15 (24) (2007) 7738–7745.
[61] J.H. Lin, M. Yamazaki, Role of P-glycoprotein in pharmacokinetics: clinical implications, Clin. Pharmacokinet. 42 (1) (2003) 59–98.
[62] C.H. Villa, D.C. Pan, S. Zaitsev, D.B. Cines, D.L. Siegel, V.R. Muzykantov, Delivery of drugs bound to erythrocytes: new avenues for an old intravascular carrier, Ther. Deliv. 6 (7) (2015) 795–826.
[63] V.R. Muzykantov, Drug delivery by red blood cells: vascular carriers designed by mother nature, Expert Opin. Drug Deliv. 7 (4) (2010) 403–427.
[64] L. Koleva, E. Bovt, F. Ataullakhanov, E. Sinauridze, Erythrocytes as carriers: from drug delivery to biosensors, Pharmaceutics 12 (3) (2020).
[65] C.E. Housecroft, E.C. Constable, An Introduction to Organic, Inorganic & Physical Chemistry, 3rd ed., Pearson Education, 2010.
[66] M.L. Friedman, K.T. Schlueter, T.L. Kirley, H.B. Halsall, Fluorescence quenching of human orosomucoid. Accessibility to drugs and small quenching agents, Biochem. J. 232 (3) (1985) 863–867.
[67] S. El-Gamel, U. Wollert, W.E. Muller, Optical studies on the specific interaction of dipyridamole with alpha 1-acid glycoprotein (orosomucoid), J. Pharm. Pharmacol. 34 (3) (1982) 152–157.